Am J Transl Res 2023;15(7):4873-4886
www.ajtr.org /ISSN:1943-8141/AJTR0148469

Original Article

Down-regulation of Jun induces senescence through destabilizing chromatin in osteoarthritis chondrocytes

Ting Xie[1*], Xunshan Ren[2*], Huangming Zhuang[2*], Fuze Jiang[2], Yuelong Zhang[2], Panghu Zhou[2]

[1]Department of Women's Health Care, Maternal and Child Health Hospital of Hubei Province, Wuhan, Hubei, China; [2]Department of Orthopedics, Renmin Hospital of Wuhan University, Wuhan, Hubei, China. [*]Equal contributors.

Received December 13, 2022; Accepted July 11, 2023; Epub July 15, 2023; Published July 30, 2023

Abstract: Objective: Osteoarthritis (OA) is the most common degenerative joint disease leading to disability worldwide. Cellular senescence is considered to be a fundamental pathogenic mechanism in the development of OA and has attracted increasing attention. However, regulatory mechanisms underlying chondrocyte senescence in OA remain unclear. Methods: Bioinformatic methods were used to screen key genes. Immunohistochemistry and the quantitative reverse transcription polymerase chain reaction were used to evaluate gene expression. RNA intervention experiments were performed to explore the functions of key genes. Results: We used 494 aging-associated genes provided by the Aging Atlas to identify the co-expression modules associated with age and OA. Thirty age-associated differentially expressed genes (ASDEGs) were identified. Using cytoHubba in Cytoscape, we identified Jun as the hub-ASDEG for OA chondrocytes. We confirmed the downregulation of Jun in OA rats and senescent chondrocytes by immunohistochemistry and quantitative reverse transcription polymerase chain reaction, respectively. Inhibition of proliferation and accelerated senescence were observed in chondrocytes treated with siRNA against Jun. Mechanistically, we observed micronuclei formation and reduced expression of H3K9me3 and heterochromatin protein 1gamma in siRNA-Jun-treated chondrocytes, indicating that destabilization of chromatin occurred during this treatment. Conclusion: Jun plays a crucial role in OA development and causes senescence by destabilizing chromatin in chondrocytes. These findings provide new insights into OA progression and suggest promising therapeutic targets.

Keywords: Osteoarthritis, senescence, chondrocyte, Jun

Introduction

Osteoarthritis (OA), characterized by articular cartilage destruction, synovial inflammation, and osteophyte formation, is one of the most common degenerative joint diseases [1]. With an aging population, the incidence of OA continues to rise worldwide, affecting almost 40% of the population over 70 years of age [2]. OA causes severe pain and disability, resulting a huge socioeconomic burden and loss of labor. However, effective treatments for OA are still lacking. Thus, exploring the pathogenesis of OA and elucidating therapeutic targets OA has become increasingly important.

Senescence is the process by which cells enter irreversible growth arrest [3]. Senescent cells accumulate with age and have been confirmed to be involved in many diseases such as Alzheimer's disease, atherosclerosis, and type 2 diabetes [4, 5]. Numerous studies have demonstrated that senescent chondrocytes accelerate the development of OA by destroying extracellular matrix homeostasis [6, 7]. The clearance of senescent chondrocytes can attenuate the development of OA and create a pro-regenerative environment [8]. Thus, uncovering the potential mechanisms underlying chondrocyte senescence is vital for OA treatment.

Weighted gene co-expression network analysis (WGCNA) is a systems biology method used to describe the relationship between sets of highly correlated genes and clinical traits [9]. WGCNA is widely used to define disease-specific gene modules in numerous tissues [10, 11]. The Aging Atlas database synthesizes large-scale gene expression and regulation datasets using

various high-throughput omics technologies to explore age-related changes in gene expression [12]. However, to the best of our knowledge, no study has used the Aging Atlas database to explore the underlying mechanisms of chondrocyte senescence in OA.

Altered chromatin structure and function contributes to cellular senescence [13]. Epigenetically, remodeled chromatin induced by histone modifications, histone tail cleavage, and exchange of histone variants affects the expression of genes associated with proliferation and longevity [14]. Thus, chromatin stability is considered an upstream factor that explains senescence.

In this study, we identified aging-associated differentially expressed genes (ASDEGs) in OA chondrocytes by combining the Aging Atlas database with WGCNA. Furthermore, we elucidated the altered expression and function of the hub-ASDEG, Jun, *in vivo* and *in vitro*. Mechanistically, we identified destabilizing chromatin as the underlying mechanism by which small interfering RNA (siRNA) against Jun induces cellular senescence. Our results reveal a novel molecule involved in chondrocyte senescence and offer a new therapeutic target for OA.

Materials and methods

Source of data

The GSE114007 dataset was downloaded from the NCBI Gene Expression Omnibus (https://www.ncbi.nlm.nih.gov/geo/) and consisted of RNA sequencing profiles from 18 normal and 20 OA human knee cartilage tissues. According to count-per-million > 1, 12,714 genes were included. The Aging Atlas (https://ngdc.cncb.ac.cn/aging/index) is a curated biomedical database comprising a range of aging-related multi-omics datasets from which we obtained and confirmed 502 aging-related genes [12].

WGCNA

The WGCNA was performed according to a previous report [15]. Briefly, we screened aging-related genes in GSE11407 and clustered the samples to exclude outliers using Pearson's correlation, with $R^2 = 0.9$ set as the screening criterion. The soft threshold = 4 was identified by constructing Soft Threshold-Scale Free Topology Model Fit and the Soft Threshold-Mean connectivity scatter plots. Subsequently, the adjacency matrix was transformed into a topological overlap matrix. Modules were identified using hierarchical clustering (minModuleSize = 10, mergeCutHeight = 0.15). The eigengenes were calculated, and the modules were hierarchically clustered. Finally, we performed Pearson's correlation analysis between the modules and clinical features (OA, age, and sex).

Functional annotation

Genes significantly associated with aging were manually annotated according to protein function using Gene Ontology (GO) and Kyoto Encyclopedia of Genes and Genomes (KEGG) enrichment analyses. The "clusterProfiler" package in the R program was used to perform functional annotation and visualization [16].

Construction of micro(mi)RNA-mRNA and transcription factor (TF)-mRNA networks

The miRNAs and TFs regulating the expression of aging-associated genes were predicted by the online databases mirWALK (http://mirwalk.umm.uni-heidelberg.de/) and ChEA3 (https://maayanlab.cloud/chea3/) [17, 18]. The results were visualized using Cytoscape software (version 3.8.2).

Protein-protein interaction (PPI) network

The Search Tool for the Retrieval of Interacting Genes (version 11.4) database was used to construct a PPI network of the screened aging-associated genes. We visualized the PPI network in the Cytoscape software and screened hub genes through the "cytoHubba" plugin.

OA rat model

Ten 8-week-old male Wistar rats were purchased from SiPeiFu Biotechnology (Beijing, China). OA was induced via anterior cruciate ligament transection (ACLT) [19]. Briefly, the rats were anesthetized with 5% isoflurane inhalation. Subsequently, the joint cavity was opened, and the anterior cruciate ligament was removed. Eight weeks after surgery, all rats were euthanized by cervical dislocation under isoflurane anesthesia and the knee joints were collected for further experiments. All experiments involving animals were conducted in

accordance with the National Research Council's Guide for the Care and Use of Laboratory Animals, and were approved by the Laboratory Animal Welfare and Ethics Committee of Renmin Hospital of Wuhan University (Approval No: 20220103A).

Histology

After fixing in 10% neutral-buffered formalin, decalcification, and embedding in paraffin, knee joints were cut into 6 μm-thick sections and stained with hematoxylin and eosin (H&E) and safranin-O/Fast Green. Cartilage destruction was scored using the Osteoarthritis Research Society International (OARSI) scoring system [20]. Immunohistochemistry was performed using rabbit anti-Jun (1:200, A0246, Abclonal, Wuhan, China) according to a previously described method [21].

Chondrocyte isolation and cultivation

Primary chondrocytes were extracted from the cartilage of 6-day-old rats. Briefly, the cartilage tissue was cut into pieces and digested for 6-8 h with 0.2% collagenase II (GC305014, Servicebio, Wuhan, China). The isolated chondrocytes were cultured in Dulbecco's modified Eagle's/F12 medium supplemented with 0.5% penicillin/streptomycin (G4003, Servicebio) and 10% fetal bovine serum (BS1618-105, BioExplorer, Boulder, CO, USA). For replicative senescence, chondrocytes were passaged at 80% confluency; passage numbers > 2 (P2) were considered senescent chondrocytes [22]. To elicit premature senescence, chondrocytes were treated with 200 μM H_2O_2 (7722-84-1, Aladdin, Shanghai, China) for 6 h [22].

β-galactosidase activity

The β-galactosidase activity assay was performed to measure cellular senescence according to the manufacturer's instructions (C0602, Beyotime, Shanghai, China). Senescent chondrocytes were counted in 3 random fields (10× magnification) using an inverted microscope.

Quantitative reverse transcription polymerase chain reaction (RT-qPCR)

Total RNA was extracted from cultured chondrocytes using a RNAeasy™ Animal RNA Isolation Kit with Spin Column (R0024, Beyotime). A SweScript RT II First Strand cDNA Synthesis Kit (G3333, Servicebio) was used to synthesize cDNA. RT-qPCR was performed using the Universal Blue SYBR Green qPCR master mix (G3326, Servicebio) in the Light Cycler® 480 II system (Roche, Basel, Switzerland) according to the manufacturer's protocol; the primer sequences are shown in Table S1. β-Actin was used as the internal control, and relative quantification was performed with the $2^{-\Delta\Delta Ct}$ method.

RNA interference

siRNA against Jun and the nonsense control (NC) were purchased from RiboBio (Guangzhou, China) and transfected using Lipofectamine 2000 (11668030, Invitrogen, Carlsbad, CA, USA) according to the manufacturer's instructions. The target sequences are listed in Table S2.

Cell viability assay

Cell viability was monitored using the Cell Counting Kit-8 (CCK8, GK10001, GlpBio, CA, USA) assay. Chondrocytes were seeded into 96-well plates (3000 cells per well) and 10 μL CCK8 reagent was added at 0, 24, 48, 72 and 96 h. Absorption at 450 nm was measured 2 h after adding the CCK8 reagent.

Colony formation assay

Chondrocytes were seeded into 6-well plates (500 cells/well) and incubated for 7-14 days under different treatments until more than 50 chondrocytes were observed in most colonies. The colonies were fixed in 4% paraformaldehyde and stained with 0.5% crystal violet for counting.

Immunofluorescence

After fixing in 4% paraformaldehyde, permeabilizing with 0.5% Triton X-100 and blocking in 10% bovine serum albumin, chondrocytes were incubated with the primary antibodies anti-Ki67 (1:200, A11390, Abclonal), heterochromatin protein 1gamma (HP1γ) (1:200, A2248, Abclonal), and H3K9me3 (1:200, A2360, Abclonal) overnight at 4°C. Next, the chondrocytes were incubated with fluorescently labeled secondary antibodies at room temperature for 2 hours. 4',6-Diamidino-2-phenylindole was used as the counterstain.

Alcian blue staining

The chondrocytes were fixed with 4% paraformaldehyde and stained with 1% (w/v) Alcian

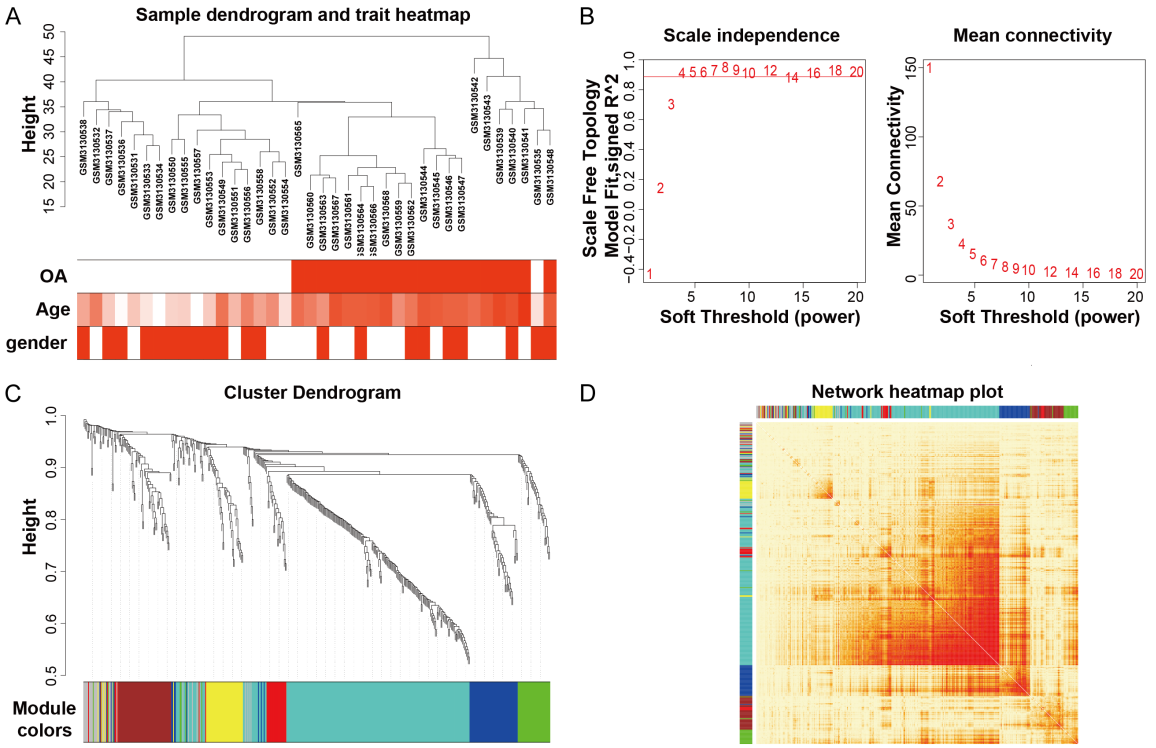

Figure 1. Construction of weighted gene co-expression network. A. Cluster analysis based on the aging-associated genes. B. Scatter plots of scale independence, mean connectivity and soft threshold. C. Cluster dendrogram of the co-expression network modules. D. The heatmap of Topological Overlap Matrix. OA, osteoarthritis.

blue (Powerful biology) for 2 h at room temperature.

Statistical analysis

All experiments were repeated independently three times and the results are presented as means ± SD. Student's t-test (two groups), one-way analysis of variance (ANOVA) followed by Bonferroni's test (multiple groups), and repeated measures ANOVA followed by Sidak's test (multiple time points) were used to test for significance. *P* value < 0.05 was considered significant. All statistical tests were 2-sided.

Results

WGCNA and identification of the aging-related model

A total of 502 reported aging-associated genes were downloaded from the Aging Atlas database and matched with 12,714 genes examined in the GSE114007 dataset. We then used the 494 matched aging-associated genes in GSE114007 to conduct the WGCNA. The cluster analysis showed that aging-associated genes could be used to divide the samples into normal and OA clusters (**Figure 1A**). Based on a scale-free R^2 = 0.9, we determined the soft-thresholding power to be 4 at which the network conformed to the power-law distribution and was closer to the real biological network state (**Figure 1B**) [10]. As shown in the clustering dendrograms, seven modules were identified (**Figure 1C**). A heatmap of the Topological Overlap Matrix was used to illustrate the co-expression networks (**Figure 1D**).

We identified the relationship between the co-expression modules and clinical traits including OA, age, and gender. As shown in **Figure 2A**, the brown module showed the strongest correlation with OA (r = 0.9, P = 7e-15) and aging (r = 0.69, P = 1e-6). The relationship between the Module Membership (MM) and Gene Significance (GS) in the brown module is shown in **Figure 2B**. Thus, 57 genes in the brown module were selected for the subsequent analysis.

Determination of differentially expressed genes (DEGs) and functional annotation

The DEG analysis was performed in GSE114007, and 1288 DEGs were determined with the threshold of P.adj ≤ 0.05 and $|\log_2 FC| \geq 1$

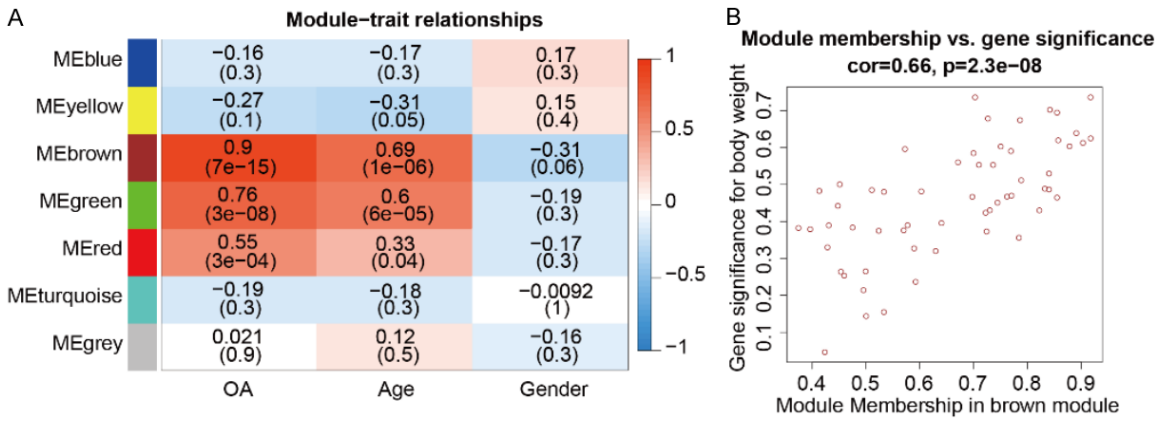

Figure 2. Identification of aging-related model. A. Heatmap of the correlation between modules and OA, age and gender. B. Scatterplot of gene significance vs. module membership in the brown module.

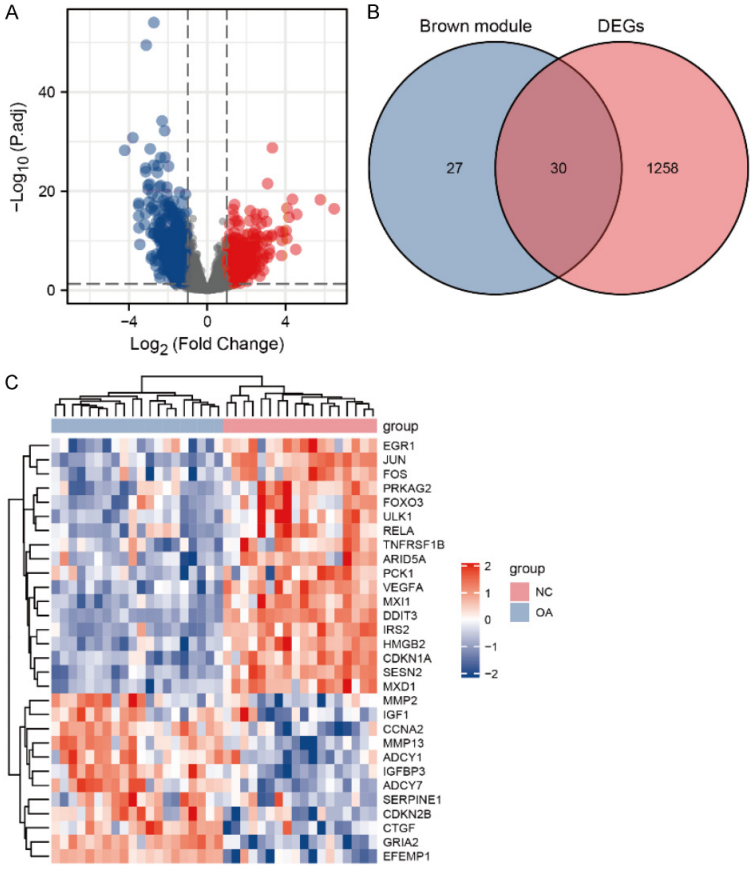

Figure 3. Determination of DEGs in the aging-related model. A. Volcano plot of DEGs in GSE114007. B. The overlap of genes in the brown module and DEGs. C. A heat map shows the expression of the ASDEGs in OA and NC groups. DEGs, differentially expressed genes; NC, negative control; OA, osteoarthritis.

(**Figure 3A**). Next, we matched the 30 DEGs in the brown module (**Figure 3B**; Table S3). The heat map shown the expression of 30 ASDEGs in the OA and normal groups (**Figure 3C**).

Next, we conducted GO and KEGG enrichment analysis to annotate the functions of ASDEGs (**Figure 4A** and **4B**). For biological processes (BP), ASDEGs were mainly involved in aging (GO:0007568, P = 8.69e-10), response to peptide hormones (GO:0043434, P = 1.26e-08), and response to starvation (GO:0042594, P = 1.36e-08). For cellular components (CC), ASDEGs were enriched in the protein kinase complex (GO:1902911, P = 5.03e-07), serine/threonine protein kinase complex (GO:1902554, P = 8.08e-06), and transferase complex, transferring phosphorus-containing groups (GO:0061695, P = 3.45e-05). The top 3 terms of molecular function (MF) enriched by ASDEGs were protein serine/threonine kinase inhibitor activity (GO:0030291, P = 1.90e-05), DNA-binding transcription repressor activity, RNA polymerase II-specific (GO:0001227, P = 4.17e-05), and DNA-binding transcription activator activity, RNA polymerase II-specific (GO:0001228, P = 6.59e-05). The KEGG pathway enrichment analysis suggested that the longevity regulating pathway (hsa04211, P = 1.81e-12), relaxin signaling pathway (hsa04926, P = 2.02e-09), and human T-cell leukemia virus 1

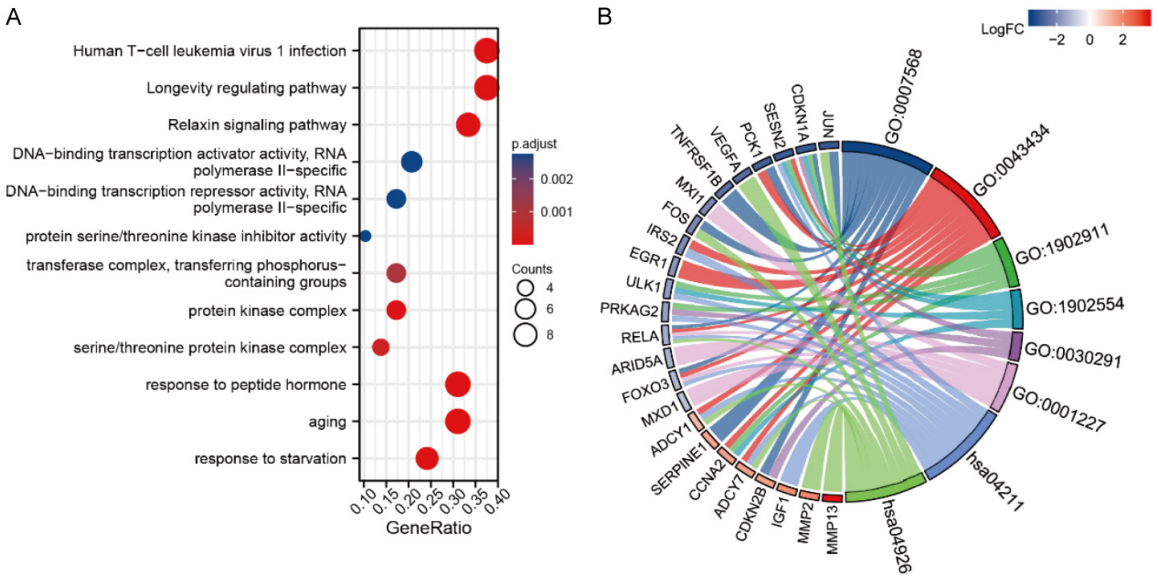

Figure 4. Functional annotation of the ASDEGs. The (A) bubble plot and the (B) chord plot of GO and KEGG results. ASDEGs, age-associated differentially expressed genes; GO, gene ontology; KEGG, Kyoto Encyclopedia of Genes and Genomes.

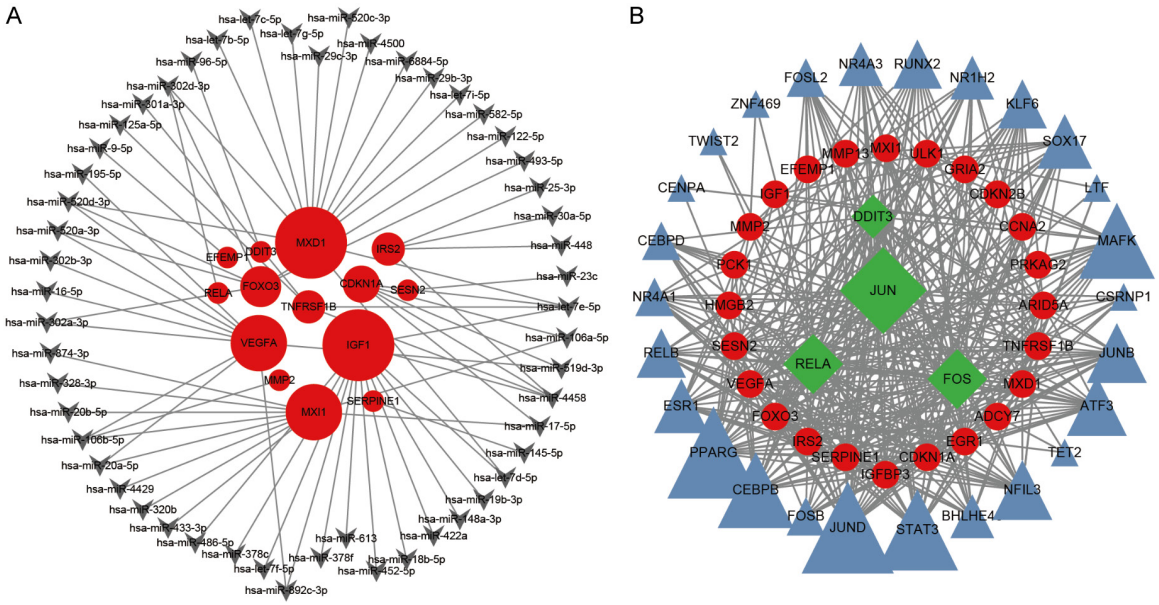

Figure 5. miRNA-ASDEGs network (A) and TF-ASDEGs network (B). The circular nodes represent the ASDEGs, triangle nodes represent TFs, and V-shaped nodes represent miRNA. miRNA, microRNA; ASDEGs, age-associated differentially expressed genes; TF, transcription factor.

infection (hsa05166, P = 6.18e-09) were the top 3 significant pathways.

Construction of miRNA-ASDEG and TF-ASDEG networks

To identify the potential regulatory molecules of ASDEGs, we constructed miRNA-ASDEG and TF-ASDEG networks (**Figure 5A** and **5B**). The networks revealed that the ASDEGs were modulated by 53 miRNAs and 30 TFs (mean rank < 100). In the miRNA-ASDEG network, MAX dimerization protein 1 and insulin-like growth factor 1 were modulated by 14 miRNAs, and 10 miRNAs modulated Mix Paired-Like Homeobox 1 and vascular endothelial growth factor A. In

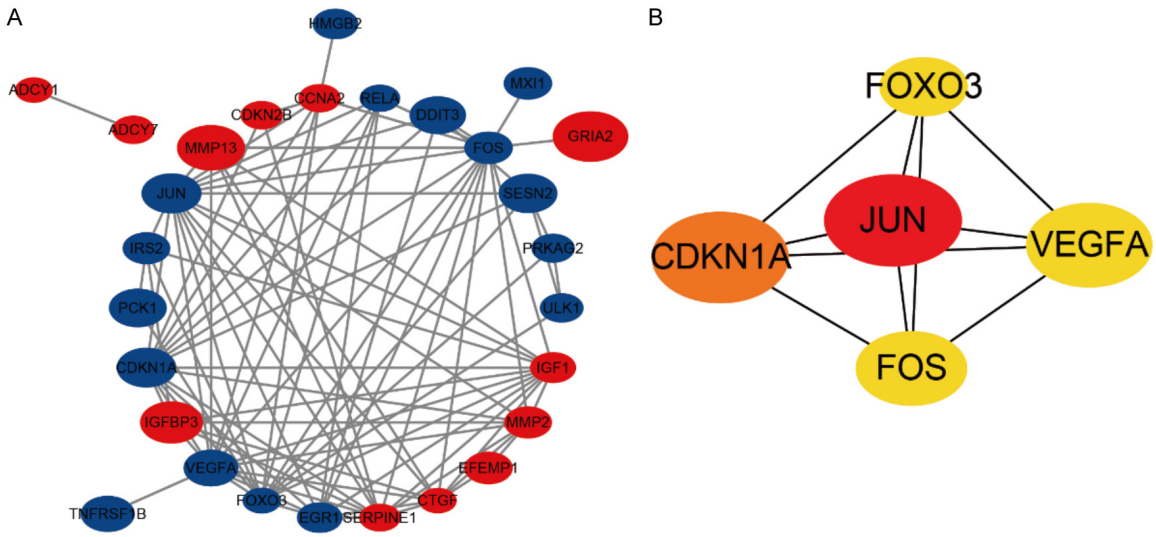

Figure 6. Construction of PPI network and identification of hub-ASDEGs. A. PPI network, blue nodes represent down-regulated ASDEGs, and red nodes represent up-regulated ASDEGs. B. The top 5 genes determined by MNC algorithm in Cytohubba. PPI, protein-protein interaction; ASDEGs, age-associated differentially expressed genes; MNC, maximum neighborhood component.

the TF-ASDEG network, JunD, peroxisome proliferation-activated receptor gamma, and Jun modulated 22, 22, and 21 ASDEGs, respectively. Concurrently, JUN, FOS, RELA and DNA damage-inducible transcript 3 acted as transcription factors that regulated the expression of other ASDEGs.

Construction of the PPI network and identification of hub-ASDEGs

The PPI network was established using ASDEGs and consisted 28 nodes and 92 interactions (**Figure 6A**). Subsequently, we utilized the "cytoHubba" package to identify the hub-ASDEGs. Because Jun was among the top three genes in eight of the 11 algorithms, we selected it as the hub-ASDEG for further validation (**Figure 6B**).

Jun was down-regulated in the cartilage of OA rats and senescent chondrocytes

To verify the relationship between Jun and OA, we established a rat ACLT-induced OA model and examined Jun expression in articular cartilage. The HE and Safranin O/Fast Green staining results indicated that ACLT destroyed the cartilage surface and reduced the OARSI scores (**Figure 7A**). Immunohistochemistry showed that the percentage of Jun-positive cells was notably reduced in OA rats (**Figure 7B**).

Next, chondrocytes were isolated from suckling rats and a duplicated senescence model was constructed to simulate senescence in an aged population. As shown in **Figure 7C**, P2 chondrocytes had a higher percentage of senescent cells than primary passage (P0) cells. The RT-qPCR results showed that Jun was significantly down-regulated in P2 chondrocytes and negatively correlated with P16 or P21, the main biomarkers of senescence (**Figure 7D**). Additionally, we treated chondrocytes with H_2O_2 to construct an oxidative stress-induced senescence model, and the same experiment was conducted with similar results (**Figure 7E** and **7F**). In summary, Jun expression was down-regulated in OA and senescent chondrocytes.

siRNA against Jun inhibited the proliferation of chondrocyte and promoted senescence

To determine the role of Jun in chondrocyte senescence, we treated chondrocytes with siRNA to suppress Jun mRNA levels (**Figure 8A**). Colony formation and CCK8 showed that the siRNA targeting Jun notably inhibited the chondrocyte proliferation (**Figure 8B** and **8C**). Immunofluorescent staining revealed a lower percentage of Ki67-positive cells in the siRNA than NC group (**Figure 8D**). Moreover, chondrocytes treated with siRNA targeting Jun showed lighter Alcian blue staining (**Figure 8E**), indicating a diminished level of extracellular matrix.

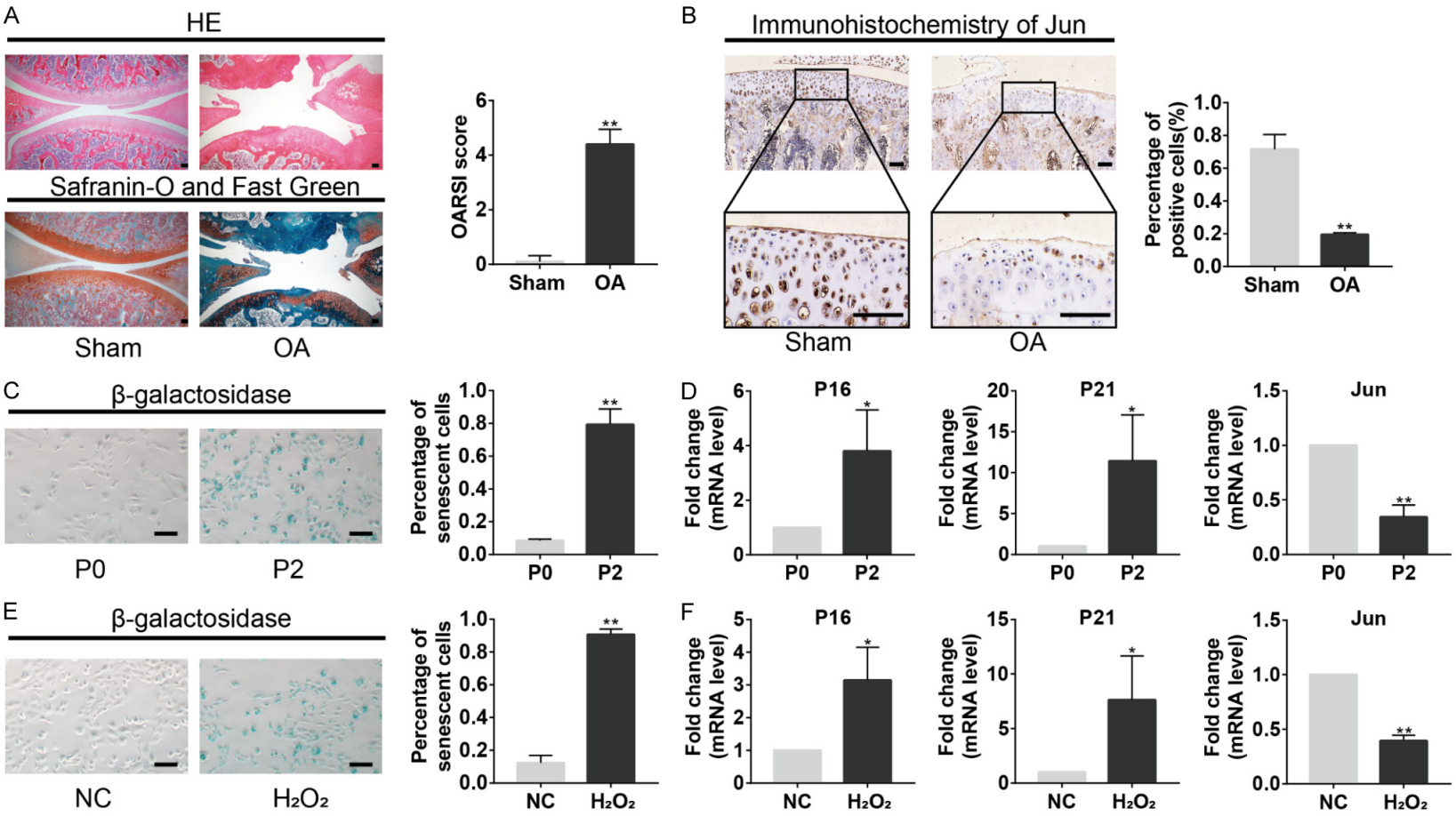

Figure 7. Jun was down-regulated in OA rat cartilage and senescent chondrocyte. A. Representative images of HE, Safranin-O/Fast Green staining of Sham and OA rat cartilage, and OARSI scores (n = 5). B. Immunohistochemistry staining of Sham and OA rat cartilage, and the percentage of Jun positive cells (n = 5). C and E. β-galactosidase activity staining and quantified results of senescent chondrocytes. D and F. qRT-PCR analysis of P16, P21 and Jun in chondrocytes. *, $P < 0.05$; **, $P < 0.01$; Scale bar: 100 μm. OA, osteoarthritis; HE, hematoxylin and eosin; OARSI, osteoarthritis research society international; qRT-PCR, quantitative reverse transcription polymerase chain reaction.

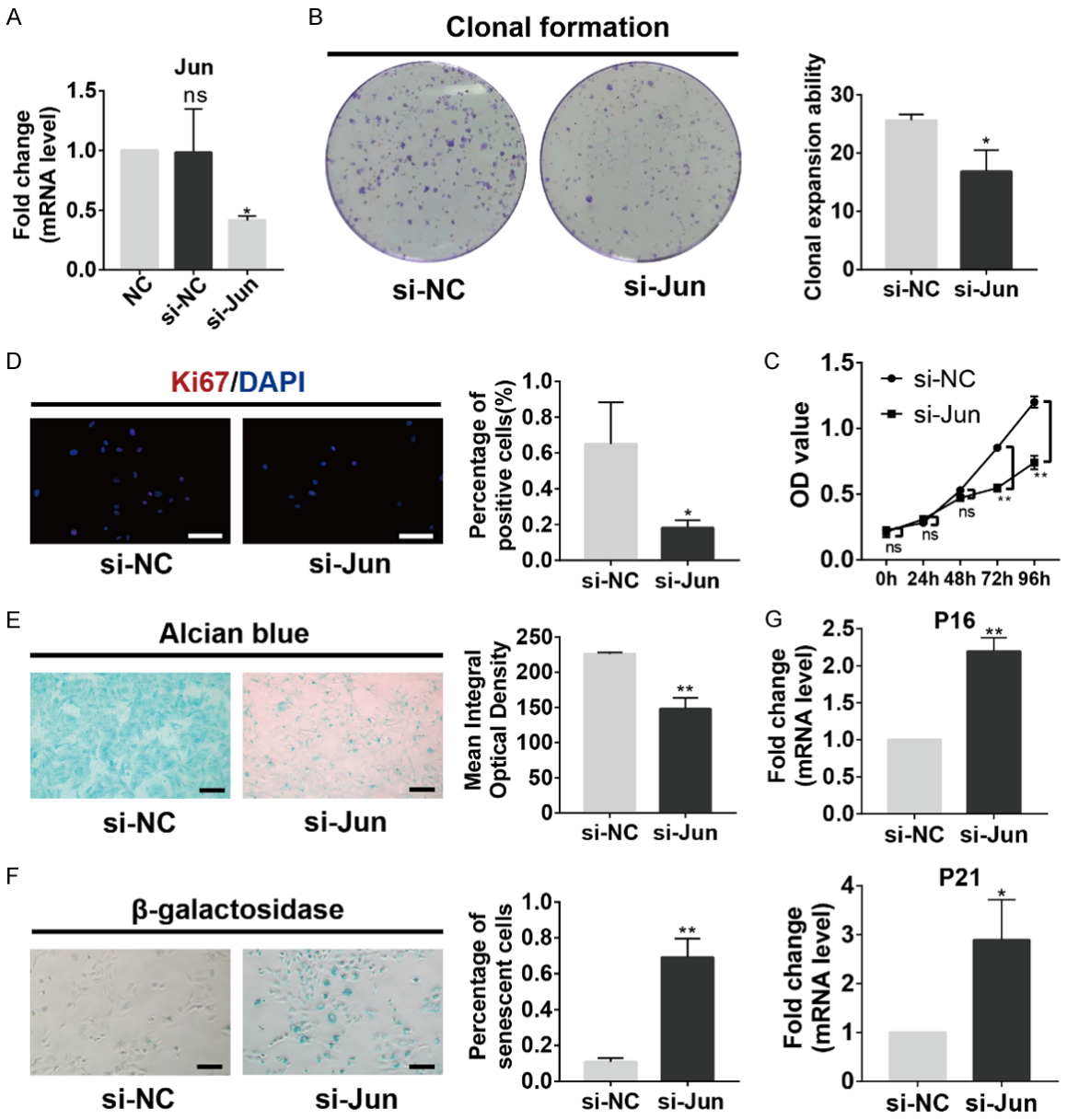

Figure 8. si-Jun inhibited the proliferation of the chondrocytes and promoted senescence. A. qRT-PCR analysis of Jun in chondrocytes exposed to si-Jun and si-NC. B. Colony formation assays in si-Jun and si-NC groups. C. CCK8 assays in si-Jun and si-NC groups. D. Representative immunofluorescence images of Ki67, and percentage of positive cells. E. Alcian blue staining assays. F. β-galactosidase activity staining and quantified results of senescent chondrocytes. G. qRT-PCR analysis of P16 and P21 in chondrocytes. *, $P < 0.05$; **, $P < 0.01$; Scale bar: 100 μm. NC, negative control; qRT-PCR, quantitative reverse transcription polymerase chain reaction; CCK8, cell counting kit-8; DAPI, 2-(4-Amidinophenyl)-6-indolecarbamidine dihydrochloride.

Subsequently, we analyzed chondrocytes senescence in the siNC and siRNA targeting Jun groups. Both the β-galactosidase staining and RT-qPCR results showed that siRNA targeting Jun induced senescence in chondrocytes (**Figure 8F** and **8G**). Thus, downregulated Jun may be the cause of chondrocytes senescence.

SiRNA targeting Jun destabilized chondrocytes chromatin

Given that changes in chromatin of senescent cells underpins the stability of the senescence phenotype, we evaluated the stability of chromatin by assessing the expression of HP1γ and H3K9me3, biomarkers of chromatin instability

[23]. The immunofluorescence results showed that treatment with siRNA against Jun caused the down-regulation of HP1γ and H3K9me3 (**Figure 9A**). Notably, siRNA against Jun resulted in micronuclei formation in interphase nuclei (**Figure 9B**). Thus, the downregulation of Jun induces senescence by destabilizing chromatin in chondrocytes.

Discussion

The incidence of OA increases with age, and imposes a substantial socioeconomic burden. Recently, cellular senescence in OA has attracted increasing research attention. Senescent cells, whether chondrocytes or synoviocytes, play a crucial role in the disease course or OA. However, underlying pathological mechanisms and molecular biomarkers remain unclear.

In this study, we sought to identify biomarkers of senescent chondrocytes in OA using the Aging Atlas database and WGCNA analysis. Combining the list of aging-related genes with clinical features of patients with OA in GSE114007, we screened 30 genes that were highly correlated with age and differentially expressed between OA and normal tissues. As expected, an enrichment analysis showed that these genes were mainly involved in aging- and longevity-regulating pathways, indicating that they were associated with senescence. Moreover, the relaxin signaling pathway and protein serine/threonine kinase inhibitor activity have been reported to be related to senescence-associated diseases [24-26]. By constructing miRNA-ASDEG and TF-ASDEG network, we confirmed that these ASDEGs were extensively regulated by miRNAs and TFs. In particular, Jun, Fos, RelA and Ddit3 regulated almost all other ASDEGs as TFs, suggesting a vital role in OA senescence. We selected Jun as the hub-ASDEGs by the cytoHubba package in Cytoscape.

Jun is a nuclear phosphoprotein that encodes a major component of the activator protein-1 (AP-1) transcription complex, one of the first mammalian transcription factors to be identified [27]. Jun can form hetero- or homodimers with members of the Jun or Fos family, which are the main subunits of AP-1. The Jun dimer binds to DNA via the TPA response element and regulates the transcription of target genes. Jun is involved in many cellular and physiological processes including proliferation, transformation, and apoptosis [28]. Recent evidence suggests that Jun plays an essential role in cellular senescence. For example, Jun inhibits the expression and function of the cell cycle regulators, P16 and P21, that are the recognized molecular regulators of senescence [29]. Furthermore, it has been reported that inhibition of Jun causes reversible proliferative arrest and withdrawal from the cell cycle [30]. Our results are consistent with these findings. We observed that a siRNA targeting Jun inhibited proliferation and promoted the expression of P16 and P21 in chondrocytes. Jun has been reported to be closely associated with chromatin remodeling [31, 32]. However, chromatin accessibility regulated by Jun remains unclear. In this work, we observed reduced expression of HP1γ and H3K9me3, and the formation of micronuclei in chondrocytes treated with siRNA against Jun, indicating that knockdown of Jun resulted in senescence by destabilizing chromatin.

Jun down-regulation has been confirmed in many senescent cell types including fibroblasts, bone marrow stromal cells and mesenchymal stem cells [33-35]. However, the expression and function of Jun/AP-1 in OA remain controversial. Gao et al. demonstrated that AP-1 was activated with interleukin (IL)-1β treatment, and inhibiting AP-1 could attenuate expression of the inflammatory cytokines, IL-6 and IL-8 [36]. Lee et al. confirmed that IL-1β production is elevated by AP-1 [37]. In addition to inflammatory cytokines, the activation of Jun regulated the secretion of matrix-degrading enzymes (e.g., matrix metalloproteinases and a disintegrin and metalloproteinase with thrombospondin motifs-5) [38, 39]. For most of these inflammatory cytokines, induction by AP-1 is essential [40]. However, Zenz et al. reported that JunB/Jun double-mutant mice developed inflammatory infiltrates in the joint regions along with bone destruction and periostitis [41]. Thus, Jun down-regulation may also contribute to OA.

Despite the lack of histological evidence, a reduced level of Jun has been suggested in transcriptomics of OA cartilage and synovium [42, 43]. In this study, we confirmed decreased Jun protein levels in ACLT-induced OA rats and senescent chondrocytes. The ultimate targets of Jun depend on the nature of the stimulus and proliferative state [44]. Therefore, Jun plays an essential role in OA chondrocyte

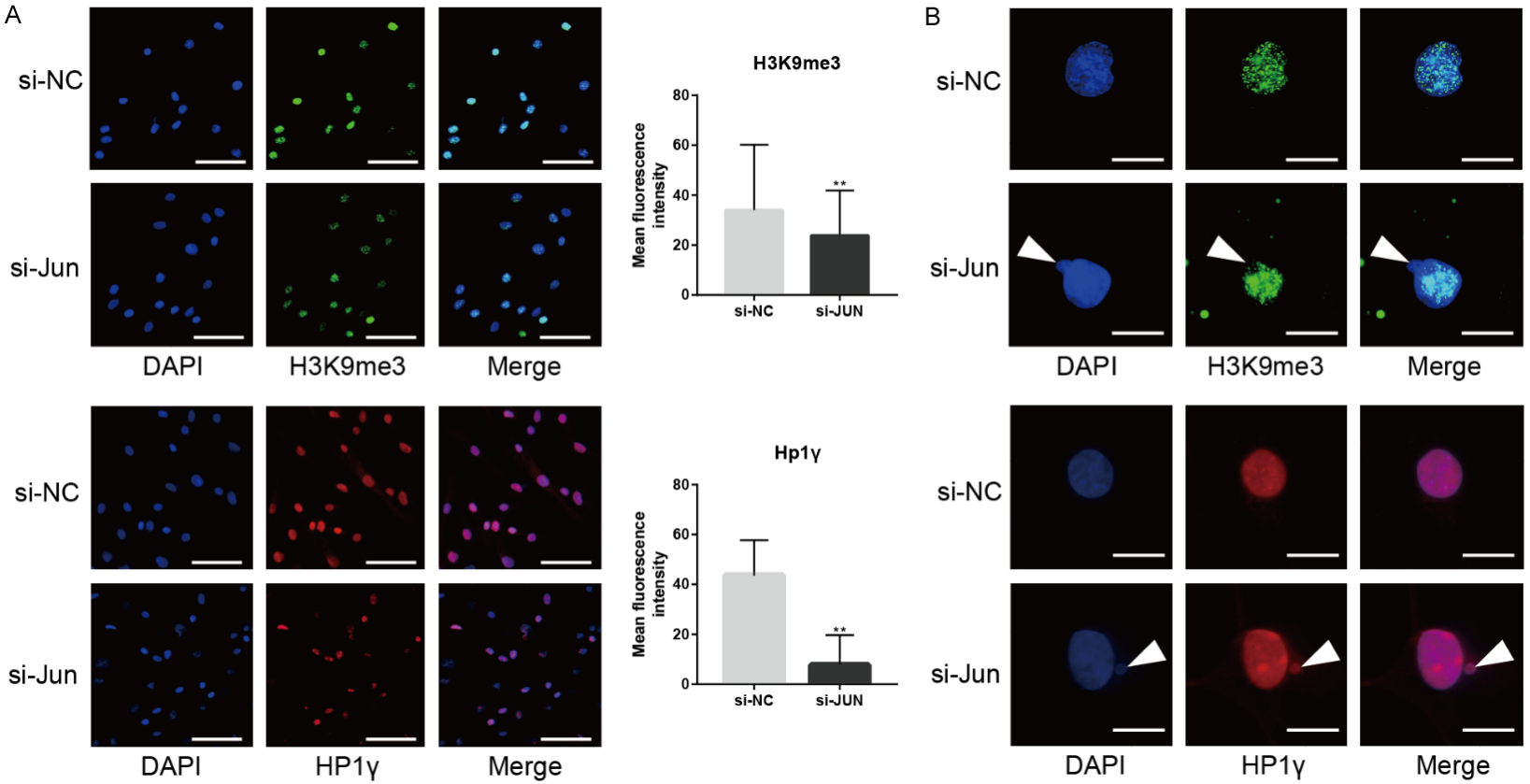

Figure 9. si-Jun destabilize chromatin of chondrocytes. A. Representative immunofluorescence images of HP1γ and H3K9me3, and mean fluorescence intensity. Scale bar: 100 μm. B. Representative immunofluorescence images of HP1γ and H3K9me3, and micronuclei formation (write arrows). Scale bar: 20 μm. **, P < 0.01. NC, negative control; DAPI, 2-(4-Amidinophenyl)-6-indolecarbamidine dihydrochloride.

senescence. However, the activity and function of Jun remain elusive, and its function in OA needs to be explored in depth.

This study has some limitations. First, owing to the unavailability of human samples, we could not assess the expression of Jun in the articular cartilage of patients with OA. Such data would be more convincing and should be obtained in the future. In addition, our study was mainly conducted at the cellular level, and the role of Jun in OA development requires further in vivo investigation. The potential mechanisms by which Jun regulates heterochromatin production and cellular senescence also require further investigation. Finally, Fos, another AP-1 subunit, was identified as an ASDEG that deserves further attention.

Conclusions

In summary, we identified Jun as the hub-ASDEG in OA chondrocytes, and confirmed that Jun expression of is reduced in OA rats and senescent chondrocytes. Moreover, we showed that downregulating Jun inhibits chondrocytes proliferation and accelerates senescence by destabilizing chromatin. Thus, Jun may serve as a novel therapeutic target for the treatment of OA.

Acknowledgements

Thanks are due to Bin Li for assistance with the valuable instruction. This work was supported by the Hubei Provincial key research and development program (No. 2021BCA147), the Cross-Innovation Talent Program of Renmin Hospital of Wuhan University (No. JCRCFZ-2022-019), and the Fundamental Research Funds for the Central Universities (No. 2042023kf0224).

Disclosure of conflict of interest

None.

Address correspondence to: Panghu Zhou, Department of Orthopedics, Renmin Hospital of Wuhan University, Wuhan, Hubei, China. E-mail: zhoupanghu@whu.edu.cn

References

[1] Huang J, Zhao L, Fan Y, Liao L, Ma PX, Xiao G and Chen D. The microRNAs miR-204 and miR-211 maintain joint homeostasis and protect against osteoarthritis progression. Nat Commun 2019; 10: 2876.

[2] Zengini E, Hatzikotoulas K, Tachmazidou I, Steinberg J, Hartwig FP, Southam L, Hackinger S, Boer CG, Styrkarsdottir U, Gilly A, Suveges D, Killian B, Ingvarsson T, Jonsson H, Babis GC, McCaskie A, Uitterlinden AG, van Meurs JBJ, Thorsteinsdottir U, Stefansson K, Davey Smith G, Wilkinson JM and Zeggini E. Genome-wide analyses using UK Biobank data provide insights into the genetic architecture of osteoarthritis. Nat Genet 2018; 50: 549-558.

[3] Omer A, Barrera MC, Moran JL, Lian XJ, Di Marco S, Beausejour C and Gallouzi IE. G3BP1 controls the senescence-associated secretome and its impact on cancer progression. Nat Commun 2020; 11: 4979.

[4] Guerrero A, De Strooper B and Arancibia-Carcamo IL. Cellular senescence at the crossroads of inflammation and Alzheimer's disease. Trends Neurosci 2021; 44: 714-727.

[5] He SH and Sharpless NE. Senescence in health and disease. Cell 2017; 169: 1000-1011.

[6] Xie J, Wang Y, Lu L, Liu L, Yu X and Pei F. Cellular senescence in knee osteoarthritis: molecular mechanisms and therapeutic implications. Ageing Res Rev 2021; 70: 101413.

[7] Loeser RF. Aging and osteoarthritis: the role of chondrocyte senescence and aging changes in the cartilage matrix. Osteoarthritis Cartilage 2009; 17: 971-979.

[8] Jeon OH, Kim C, Laberge RM, Demaria M, Rathod S, Vasserot AP, Chung JW, Kim DH, Poon Y, David N, Baker DJ, van Deursen JM, Campisi J and Elisseeff JH. Local clearance of senescent cells attenuates the development of post-traumatic osteoarthritis and creates a pro-regenerative environment. Nat Med 2017; 23: 775-781.

[9] Langfelder P and Horvath S. WGCNA: an R package for weighted correlation network analysis. BMC Bioinformatics 2008; 9: 559.

[10] Yang Q, Wang R, Wei B, Peng C, Wang L, Hu G, Kong D and Du C. Candidate biomarkers and molecular mechanism investigation for glioblastoma multiforme utilizing WGCNA. Biomed Res Int 2018; 2018: 4246703.

[11] Zhang X, Cui Y, Ding X, Liu S, Han B, Duan X, Zhang H and Sun T. Analysis of mRNA-lncRNA and mRNA-lncRNA-pathway co-expression networks based on WGCNA in developing pediatric sepsis. Bioengineered 2021; 12: 1457-1470.

[12] Liu GH, Bao YM, Qu J, Zhang WQ, Zhang T, Kang W, Yang F, Ji QZ, Jiang XY, Ma YK, Ma S, Liu ZP, Chen SY, Wang S, Sun SH, Geng LL, Yan KW, Yan PZ, Fan YL, Song MS, Ren J, Wang QR, Yang SS, Yang YH, Xiong MZ, Liang CQ, Li LZ,

Cao TL, Hu JL, Yang P, Ping JL, Hu HF, Zheng YD, Sun GQ, Li JM, Liu LX, Zou ZR, Ding YJ, Li MH, Liu D, Wang M, Sun XY, Wang C, Bi SJ, Shan HZ and Zhuo X; Aging Atlas Consortium. Aging atlas: a multi-omics database for aging biology. Nucleic Acids Res 2021; 49: D825-D830.

[13] Baumann C, Zhang X and De La Fuente R. Loss of CBX2 induces genome instability and senescence-associated chromosomal rearrangements. J Cell Biol 2020; 219: e201910149.

[14] Sen P, Shah PP, Nativio R and Berger SL. Epigenetic mechanisms of longevity and aging. Cell 2016; 166: 822-839.

[15] Tian Z, He W, Tang J, Liao X, Yang Q, Wu Y and Wu G. Identification of important modules and biomarkers in breast cancer based on WGCNA. Onco Targets Ther 2020; 13: 6805-6817.

[16] Yu G, Wang LG, Han Y and He QY. clusterProfiler: an R package for comparing biological themes among gene clusters. OMICS 2012; 16: 284-287.

[17] Sticht C, De La Torre C, Parveen A and Gretz N. miRWalk: an online resource for prediction of microRNA binding sites. PLoS One 2018; 13: e0206239.

[18] Keenan AB, Torre D, Lachmann A, Leong AK, Wojciechowicz ML, Utti V, Jagodnik KM, Kropiwnicki E, Wang Z and Ma'ayan A. ChEA3: transcription factor enrichment analysis by orthogonal omics integration. Nucleic Acids Res 2019; 47: W212-W224.

[19] Liao CR, Wang SN, Zhu SY, Wang YQ, Li ZZ, Liu ZY, Jiang WS, Chen JT and Wu Q. Advanced oxidation protein products increase TNF-alpha and IL-1 beta expression in chondrocytes via NADPH oxidase 4 and accelerate cartilage degeneration in osteoarthritis progression. Redox Biol 2020; 28: 101306.

[20] Glasson SS, Chambers MG, Van den Berg WB and Little CB. The OARSI histopathology initiative - recommendations for histological assessments of osteoarthritis in the mouse. Osteoarthritis Cartilage 2010; 18 Suppl 3: S17-S23.

[21] Sun X, Chuang JC, Kanchwala M, Wu L, Celen C, Li L, Liang H, Zhang S, Maples T, Nguyen LH, Wang SC, Signer RA, Sorouri M, Nassour I, Liu X, Xu J, Wu M, Zhao Y, Kuo YC, Wang Z, Xing C and Zhu H. Suppression of the SWI/SNF component Arid1a promotes mammalian regeneration. Cell Stem Cell 2016; 18: 456-466.

[22] Kang D, Shin J, Cho Y, Kim HS, Gu YR, Kim H, You KT, Chang MJ, Chang CB, Kang SB, Kim JS, Kim VN and Kim JH. Stress-activated miR-204 governs senescent phenotypes of chondrocytes to promote osteoarthritis development. Sci Transl Med 2019; 11: eaar6659.

[23] Nelson DM, Jaber-Hijazi F, Cole JJ, Robertson NA, Pawlikowski JS, Norris KT, Criscione SW, Pchelintsev NA, Piscitello D, Stong N, Rai TS, McBryan T, Otte GL, Nixon C, Clark W, Riethman H, Wu H, Schotta G, Garcia BA, Neretti N, Baird DM, Berger SL and Adams PD. Mapping H4K20me3 onto the chromatin landscape of senescent cells indicates a function in control of cell senescence and tumor suppression through preservation of genetic and epigenetic stability. Genome Biol 2016; 17: 158.

[24] Martin G, Bogdanowicz P, Domagala F, Ficheux H and Pujol JP. Rhein inhibits interleukin-1 beta-induced activation of MEK/ERK pathway and DNA binding of NF-kappa B and AP-1 in chondrocytes cultured in hypoxia: a potential mechanism for its disease-modifying effect in osteoarthritis. Inflammation 2003; 27: 233-246.

[25] Leysen H, Walter D, Clauwaert L, Hellemans L, van Gastel J, Vasudevan L, Martin B and Maudsley S. The relaxin-3 receptor, RXFP3, is a modulator of aging-related disease. Int J Mol Sci 2022; 23: 4387.

[26] Arbones ML, Thomazeau A, Nakano-Kobayashi A, Hagiwara M and Delabar JM. DYRK1A and cognition: a lifelong relationship. Pharmacol Ther 2019; 194: 199-221.

[27] Angel P and Karin M. The role of Jun, Fos and the Ap-1 complex in cell-proliferation and transformation. Biochim Biophys Acta 1991; 1072: 129-157.

[28] Bejjani F, Evanno E, Zibara K, Piechaczyk M and Jariel-Encontre I. The AP-1 transcriptional complex: local switch or remote command? Biochim Biophys Acta Rev Cancer 2019; 1872: 11-23.

[29] Shaulian E and Karin M. AP-1 as a regulator of cell life and death. Nat Cell Biol 2002; 4: E131-E136.

[30] Smith MJ and Prochownik EV. Inhibition of C-Jun causes reversible proliferative arrest and withdrawal from the cell cycle. Blood 1992; 79: 2107-2115.

[31] Lv X, Li Q, Liu H, Gong M, Zhao Y, Hu J, Wu F and Wu X. Jun activation modulates chromatin accessibility to drive TNF alpha-induced mesenchymal transition in glioblastoma. J Cell Mol Med 2022; 26: 4602-4612.

[32] Milavetz BI. SP1 and AP-1 elements direct chromatin remodeling in SV40 chromosomes during the first 6 hours of infection. Virology 2002; 294: 170-179.

[33] Li Y, Zeng N, Qin Z, Chen Y, Lu Q, Cheng Y, Xia Q, Lu Z, Gu N and Luo D. Correction: ultrasmall prussian blue nanoparticles attenuate UVA-induced cellular senescence in human dermal fibroblasts via inhibiting the ERK/AP-1 pathway. Nanoscale 2022; 14: 7943.

[34] Tohjima E, Inoue D, Yamamoto N, Kido S, Ito Y, Kato S, Takeuchi Y, Fukumoto S and Matsumoto

T. Decreased AP-1 activity and interleukin-11 expression by bone marrow stromal cells may be associated with impaired bone formation in aged mice. J Bone Miner Res 2003; 18: 1461-1470.

[35] Tome M, Sepulveda JC, Delgado M, Andrades JA, Campisi J, Gonzalez MA and Bernad A. miR-335 correlates with senescence/aging in human mesenchymal stem cells and inhibits their therapeutic actions through inhibition of AP-1 activity. Stem Cells 2014; 32: 2229-2244.

[36] Gao YX, Yu HH, He C, Li M, Guo DD, Lian JJ, Yang HJ, Wang M, Wang L, Feng ZW and Cheng BF. Fengshi gutong capsule attenuates osteoarthritis by inhibiting MAPK, NF-kappa B, AP-1, and Akt pathways. Front Pharmacol 2018; 9: 910.

[37] Lee KT, Chen BC, Liu SC, Lin YY, Tsai CH, Ko CY, Tang CH and Tung KC. Nesfatin-1 facilitates IL-1 beta production in osteoarthritis synovial fibroblasts by suppressing miR-204-5p synthesis through the AP-1 and NF-kappa B pathways. Aging (Albany NY) 2021; 13: 22490-22501.

[38] Ji Q, Xu X, Zhang Q, Kang L, Xu Y, Zhang K, Li L, Liang Y, Hong T, Ye Q and Wang Y. The IL-1 beta/AP-1/miR-30a/ADAMTS-5 axis regulates cartilage matrix degradation in human osteoarthritis. J Mol Med (Berl) 2016; 94: 771-785.

[39] Liacini A, Sylvester J, Li WQ and Zafarullah M. Inhibition of interleukin-1-stimulated MAP kinases, activating protein-1 (AP-1) and nuclear factor kappa B (NF-kappa B) transcription factors down-regulates matrix metalloproteinase gene expression in articular chondrocytes. Matrix Biol 2002; 21: 251-262.

[40] Zenz R, Eferl R, Scheinecker C, Redlich K, Smolen J, Schonthaler HB, Kenner L, Tschachler E and Wagner EF. Activator protein 1 (Fos/Jun) functions in inflammatory bone and skin disease. Arthritis Res Ther 2008; 10: 201.

[41] Zenz R, Eferl R, Kenner L, Florin L, Hummerich L, Mehic D, Scheuch H, Angel P, Tschachler E and Wagner EF. Psoriasis-like skin disease and arthritis caused by inducible epidermal deletion of Jun proteins. Nature 2005; 437: 369-375.

[42] Fisch KM, Gamini R, Alvarez-Garcia O, Akagi R, Saito M, Muramatsu Y, Sasho T, Koziol JA, Su AI and Lotz MK. Identification of transcription factors responsible for dysregulated networks in human osteoarthritis cartilage by global gene expression analysis. Osteoarthritis Cartilage 2018; 26: 1531-1538.

[43] Xia L and Gong N. Identification and verification of ferroptosis-related genes in the synovial tissue of osteoarthritis using bioinformatics analysis. Front Mol Biosci 2022; 9: 992044.

[44] Hess J, Angel P and Schorpp-Kistner M. AP-1 subunits: quarrel and harmony among siblings. J Cell Sci 2004; 117: 5965-5973.

Table S1. Primer sequences used in this study

Gene	F/R	Sequence
β-actin	F	5'-TGCTATGTTGCCCTAGACTTCG-3'
	R	5'-GTTGGCATAGAGGTCTTTACGG-3'
Jun	F	5'-GAACTGCATAGCCAGAATACGCTG-3'
	R	5'-GCGCTTTCAAGGTTTTCACTTTTT-3'
P16	F	5'-GAGGACCCCACCACCCTCTC-3'
	R	5'-ATACCGCAAATACCGCACGA-3'
P21	F	5'-CTTTCTTTGTGTATTTGCCA-3'
	R	5'-AACTCCTGAGCCTGTTTCGT-3'

Abbreviations: F, forward; R, reverse.

Table S2. Primer sequences used in this study

siRNA name	Target sequences
si-r-Jun	GGCACAGCTTAAACAGAAA

Abbreviations: siRNA, small interfering RNA.

Table S3. The list of age-related genes and ASDEGs

	Gene name
Age-related genes	VEGFC GRIA2 ARNTL ATP5O AXL BLM FOXL2 BRCA2 C1QA CD9 CEBPA CETP ERCC8 CLU CNR1 CSF2RB CTGF CD55 DBN1 DLAT EEF1A1 EEF2 EMD EPS8 ERCC1 ERCC2 ERCC3 ERCC4 ERCC5 ERCC6 ESR1 EFEMP1 FEN1 FLT1 XRCC6 GCLC GCLM GPX1 GPX4 GRN NR3C1 GSK3A GSR GSS GSTA4 GSTP1 GTF2H2 H2AFX HTT HELLS NRG1 HIC1 HMGB2 HOXB7 HOXC4 HSF1 HSPA9 HSPD1 IGFBP1 IGFBP2 KCNA3 FADS1 LRP2 MXD1 MIF MLH1 MMP10 MMP12 MSRA MT1E MT-CO1 NUDT1 MXI1 NFE2L1 NFE2L2 PRDX1 PAPPA PCMT1 ARID5A SPRTN SIRT2 RAD27 TMEM67 NLRP3 CISD2 MMP14 BMP2 BMP6 SP1 NOG MVK BMI1 TCF3 HESX1 CALR BRCA1 ELN HGF HSP90AA1 ITGA2 RET PTEN IL2 IL2RG IL7 IL7R LEP LEPR FBP1 GCK GRB2 GSK3B IKBKB PCK1 PDPK1 PPP1CA MAPK3 MAPK8 MAPK9 PTPN1 SHC1 SOCS2 CEBPB MMP1 MMP3 MMP13 CREBBP ENO1 ENO2 GAPDH HIF1A HK3 TIMP1 VEGFA PLCG2 POU1F1 PTK2 SST SSTR3 STAT3 STAT5A STAT5B EP300 FOS GH1 GHR GHRH GHRHR JAK2 EGR1 PTK2B PIGF PSAT1 FOXO4 MMP2 IL2RB IL6ST IL15 TNFRSF11B TNFRSF1B TNFRSF10C PLAUR SERPINB2 RORA RB1 TGFB1 SQSTM1 CCNA2 CDKN2B MAPK14 E2F1 FOXM1 IL6 CXCL8 MYC NBN ABL1 BUB1B CDK7 HDAC1 HDAC2 PCNA PRKDC TFDP1 YWHAZ BUB3 PECAM1 MYLK HMGB1 PRKCD AIFM1 HTRA2 BAK1 LMNA LMNB1 DCTN1 AARS1 APOE APP IL1A SDHC TNFRSF1A MYD88 NFKB2 NGF NGFR PDGFB PDGFRA PDGFRB ADCY1 ADCY2 ADCY3 ADCY5 ADCY6 ADCY7 ADCY8 ADCY9 AKT1 AKT2 ATF4 BAX CAMK4 CAT CREB1 ATF2 ATF6B EIF4E EIF4EBP1 FOXO1 FOXO3 MTOR HRAS IGF1 IGF1R INS INSR IRS1 NFKB1 NRAS SESN3 IRS4 EIF4E1B ADCY4 CREB3L4 EHMT1 CREB3L1 CREB3L3 AKT1S1 SESN2 PIK3CA PIK3CB PIK3CD PIK3R1 PIK3R2 PPARG PRKAA1 PRKAA2 PRKAB1 PRKAB2 PRKACA PRKACB PRKACG PRKAG1 RELA RHEB RPS6KB1 RPS6KB2 SOD2 STK11 TP53 TSC1 TSC2 ULK1 KRAS PIK3R3 IRS2 KL ADIPOQ EIF4E2 ATG5 CREB5 ATG13 RB1CC1 AKT3 CREB3 CAMKK2 PPARGC1A EHMT2 SIRT1 APPL1 SESN1 ADIPOR1 PRKAG2 PRKAG3 RPTOR ATG101 CREB3L2 ADIPOR2 PTPN11 CTF1 EPOR IFNB1 TP73 PPM1D CHEK2 CYCS FAS ATM ATR BCL2 CDK1 CDKN1A CDKN2A IGFBP3 MDM2 SERPINE1 NCOR2 DLL3 PLAU PLCG1 PRKCB PRKCQ RELB CCL4 CCL13 CCL19 CCL21 CXCL12 SYK MAP3K7 TLR4 TNFAIP3 TRAF1 TRAF2 TRAF3 TRAF6 VCAM1 ZAP70 TRIM25 IKBKG TNFSF11 TRADD RIPK1 TNFSF14 TNFRSF11A CFLAR BCL10 MAP3K14 TAB1 TNFSF13B TAB2 DDX58 CARD10 PIAS4 PIDD1 PARP1 BIRC2 BIRC3 XIAP BCL2A1 BCL2L1 BTK CD14 CD40LG CXCL1 CXCL2 IL1R1 NFKBIA TIRAP TNFRSF13C EDARADD TICAM1 RICTOR PRKCA TNF WNT2 UBB PTGES FGF23 RPS6KA5 FGF21 AR AREG BDNF CACNA1A CDC42 DDIT3 EGF EGFR ERBB2 FGF7 FGFR1 FGFR3 HSPA1A HSPA1B HSPA8 IGF2 IL1B JUND MAPT MAX MAP3K5 PSEN1 CSNK1E CTNNB1 JUN MMP7 PTGS2 PIN1 PMCH PML POLA1 POLB POLD1 POLG PON1 PPARA MED1 PROP1 PEX5 PYCR1 RAD51 RAD52 RFC4 RPA1 S100B CCL1 CCL3 CCL7 CCL20 CXCL6 CXCL5 SLC13A1 SNCG SOD1 TAF1 TBP TERC TERF1 TERF2 TERT TFAP2A TIMP2 TOP1 TOP2A TOP2B TP53BP1 TPP2 TRPS1 TXN UBE2I SUMO1 UCHL1 UCP1 UCP2 UCP3 VCP TRPV1 WRN XPA XRCC5 RAE1 TP63 DGAT1 HDAC3 TOP3B RGN KCNAB3 RECQL4 GDF15 EEF1E1 CLOCK NCOR1 TRAP1 TOPORS GDF11 COQ7 ZMPSTE24 STUB1 CCL26 RACK1 AGPAT2 SUN1 SIRT3 CBX7 SIN3A BSCL2 HBP1 CHCHD2 SIRT7 SIRT6 APTX EIF5A2 A2M ADH1B ADH5 AGTR1 ALDH2 ALDH9A1 APEX1 APOC3 ARHGAP1
ASDEGs	DDIT3 SESN2 JUN GRIA2 CDKN1A VEGFA IRS2 HMGB2 MXI1 MXD1 MMP13 IGFBP3 ULK1 ADCY7 PCK1 PRKAG2 TNFRSF1B CCNA2 FOS RELA EFEMP1 EGR1 FOXO3 ARID5A CDKN2B MMP2 CTGF ADCY1 IGF1 SERPINE1

Abbreviations: ASDEGs, age-associated differentially expressed genes.